Vision, Modeling, and Visualization (2011)
Peter Eisert, Konrad Polthier, and Joachim Hornegger (Eds.)

AFiT - Atrial Fibrillation Ablation Planning Tool

A. Brost [1], F. Bourier [2], A. Kleinoeder [1], J. Raab [3], M. Koch [1], M. Stamminger [3], J. Hornegger [1], N. Strobel [4], K. Kurzidim [2]

[1] Pattern Recognition Lab, Friedrich-Alexander-University Erlangen-Nuremberg, Erlangen, Germany
[2] Klinik für Herzrhythmusstörungen, Krankenhaus Barmherzige Brüder, Regensburg, Germany
[3] Computer Graphics Group, Friedrich-Alexander-University Erlangen-Nuremberg, Erlangen, Germany
[4] Siemens AG, Forcheim, Germany

Abstract

The planning of cryo-balloon ablations for treatment of atrial fibrillation is a crucial task for a physician as he has to determine which size of the balloon catheter is required for isolation at each pulmonary vein. Today, the diameter of the pulmonary vein's ostium is measured in a pre-operative data set to determine which type of catheter is most appropriate. We present a novel tool that visualizes a cryo-balloon catheter model within a 3-D model representing a segmented left atrium. Using this approach, physicians are able to better assess the catheter fit. So far, measurement of the pulmonary vein diameters have been performed by evaluation of 2-D slices taken from pre-operative data sets. The first feedback obtained by physicians was very encouraging as this tool offers better insights for balloon catheter ablation procedures.

Categories and Subject Descriptors (according to ACM CCS): I.3.7 [Computer Graphics]: Three-Dimensional Graphics and Realism—Virtual Reality

1. Introduction

Atrial fibrillation (AFib) is widely recognized the most common heart arrhythmia [CBP*07, CAMO11]. It is also on top of the list of diseases that are considered as a leading cause of stroke [GWS*01, WAK91, FR11]. The first-line of treatment for AFib today is drug therapy. If drug therapy fails, then the second-line treatment option is electrical isolation of the pulmonary veins (PVs) attached to the left atrium [CBP*07, BHS*11, BSG*11, BSH*11]. The current minimally-invasive approaches typically rely on radio-frequency ablation catheters [HGF*94] or on cryo-balloon catheters [AUR*03, VJR*07]. The cryo-balloon ablation technique was introduced to reduce risks related to radio-frequency catheter ablation such as pulmonary vein stenosis and esophageal fistula [DKCJ11, NVS*08, BBY*10]. If balloon catheters fit well to the anatomy of the left atrium, a contiguous circular lesion can be achieved very efficiently, thus, simplifying the procedure and speeding it up as well. Catheter ablation procedures are performed in electrophysiology (EP) labs usually equipped with modern C-arm X-ray systems providing 3-D imaging of the heart [PHL*09]. Augmented fluoroscopy using a perspectively forward projected overlay representation of 3-D objects onto live fluoroscopic images has become a useful tool for navigation when performing ablation procedures [DME*05, EDH*08, EDDL*08, BWL*11]. Unfortunately, current navigation tools do not provide tools to localize and visualize cryo-balloon catheters in 3-D. Commercially available cryo-balloons come in two different diameters, a 23 mm balloon and a 28 mm balloon [FO11]. It mainly depends on the patients anatomy, espacially the configuration of the left atrium and the pulmonary veins, which balloon to choose. Different methods are proposed how to assess which balloon should be used depending on measurements in pre-operative data sets. Most of the time, only the diameter of the pulmonary vein is estimated, see Fig. 1 for an example. This measurement is cumbersome, and it may even be misleading. We propose the first method to assess 3-D cryo-balloon positions within a pre-operative 3-D data set. Using our proposed method, we can provide information to the physician which catheter size is more likely to fit.

In the first section of this paper, we briefly describe the standard procedure to determine the diameter of the pulmonary veins. In the second, we introduce our new approach

DOI: 10.2312/PE/VMV/VMV11/223-230

using our atrial fibrillation ablation planning tool. In the last section we discuss the advantages and disadvantages of our approach.

2. Default Assessment

A pre-operative data set is required to assess which cryo-balloon catheter type can be used. Commercially available products such as *syngo* InSpace EP (Siemens AG, Healthcare Sector, Forchheim, Germany) are capable of segmenting the left atrium in pre-operative data sets such as CT [BBLP10], MRI [MHB*03] or C-Arm CT [PHL*09, BSY*09a, SMB*09, BSY*09b], see Fig. 2 for a segmented MRI. This segmentation can also be used to determine the diameter of the ostium of the pulmonary veins. The assessment can be performed by using the combination of the segmentation and the pre-operative data set, see Fig. 3. Recently *'the ratio between the maximal and minimal PV ostial diameter and the angle between the PV longitudinal and the frontal body axis'* has been proposed to assess which balloon has to be chosen [FO11]. But this increases the time required for a physician to determine which catheters are required during the procedure. To reduce the amount of a physician's time required for the assessment and to provide a better visual feedback, we propose to use the segmented left atrium which is visualized in 3-D and to place a 23 mm and/or a 28 mm balloon catheter at the ostium of the pulmonary vein to visually perform the assessment.

3. AFiT

In this section, we summarize the **A**trial **Fi**brillation Ablation Planning **T**ool. First, the visualization methods for the left atrium and the cryo-balloon are explained. Afterwards, some details on the positioning of the balloon and the carving view are presented.

3.1. Object Visualization

Left Atrium Visualization is achieved by loading and displaying a segmented 3-D mesh of the left atrium (LA). In our case, *syngo* InSpace EP (Siemens AG, Healthcare Sector, Forchheim, Germany) was used for segmentation. For testing of our software prototype, an MRI volume data set with 63 slices and a matrix size of 256×256 was used. Each voxel of the volume was of size $1.03\text{mm} \times 1.03\text{mm} \times 1.62\text{mm}$ and was represented by 9 Bit. The segmentation result is stored as indexed face set in a .xml format. The .xml file contains information about the position of the object's vertices and normals. Additionally, topological information about which vertices build a triangle is stored. To be able to display the segmented LA, the indexed face set was read out from the file and stored to a vertex-buffer-object (VBO). VBO's combine the benefits of vertex-lists and display lists. The geometry information stored in an VBO is fast accessible and easy to update [AHH08]. Depending on the usage of the data, the memory manager can optimize the access and storage of the data. Static data, e.g., that is not changing can be stored directly in the high speed memory of the graphics-card. By doing so, large objects can be drawn very fast and further extension of the tool can easy be realized. To place the LA around the origin, the position of each vertex was translated by the mean of all vertices. Our tool provides the method to freely rotate the left atrium and also to zoom in and out. This visualization is represented in Fig. 4.

Cryo-Balloon Visualization is performed by using a sphere with a diameter of either 23 mm or 28 mm as catheter model. These sizes represent the available cryo-balloon diameters of the Arctic Front device (Medtronic CryoCath, Pointe-Claire, Quebec, Canada). The cryo-balloon models can be freely moved around and be positioned at the ostium of the pulmonary veins. To position the catheter, the catheter model needs to be selected and is then moved parallel to the viewing direction. Hence, our tool requires a rotation of the view to reach the desired position. By doing so, we make sure that our software is easy to use and the user is required to look from different positions at the left atrium. The balloon automatically occludes the mesh representing the left atrium. The position of the cryo-balloon with respect to the LA can be stored and loaded upon request. An example for the visualization is given in Fig. 5.

Transparency is achieved by changing the opacity of triangles that are facing towards the camera. Those triangles that are facing away from the observer are not changed. By doing so, we avoid that the left atrium is faded to black. Besides changing the transparency we provide a carving view. Carving means, that the front face of the left atrium is partially invisible to a certain degree. In the past years, the use of shaders has evolved to an established method in computer graphics because they provide a huge flexibility. Nowadays shaders are available and visualization pipelines do not need to comply with a standard rendering pipeline. More information about shader can be found in [RLG*09]. To achieve a correct visualization of transparency, some drawing aspects have to be considered [WHSL10]. First of all, the LA has to be divided into two parts, one which consists of all back facing polygons, and one comprising all front facing polygons. The back facing part is usually not visible to the viewer. However, if the front becomes transparent or is cut out, the back face of the object will be visible as well. To this end, blending has to be enabled [Shr09]. During blending, the color of already drawn primitives is combined with the color of the incoming primitive which then results in a translucent looking material. An example of the visualization is given in Fig. 7 (a).

3.2. Carving View

In the following section, a vertex $\mathbf{p}$ is considered as a point that is used to generate the mesh in 3-D, whereas a pixel $\mathbf{q}$ is considered as an interpolated 3-D point on the mesh which

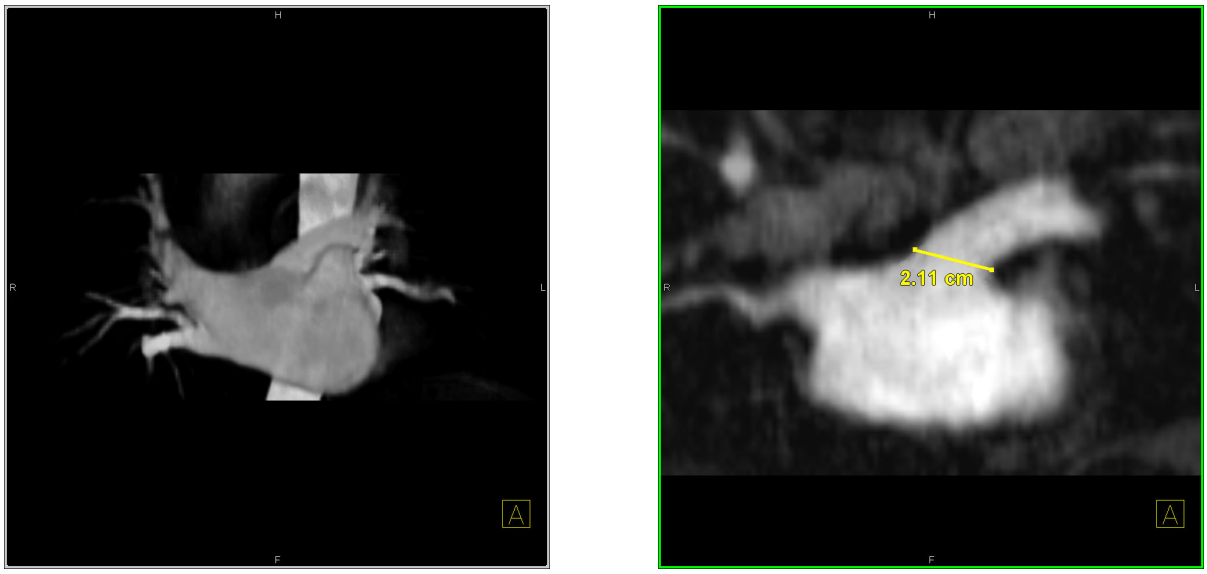

(a) (b)

Figure 1: *(a) MRI volume data of the left atrium (b) Manual measurement of the diameter of the left superior pulmonary vein.*

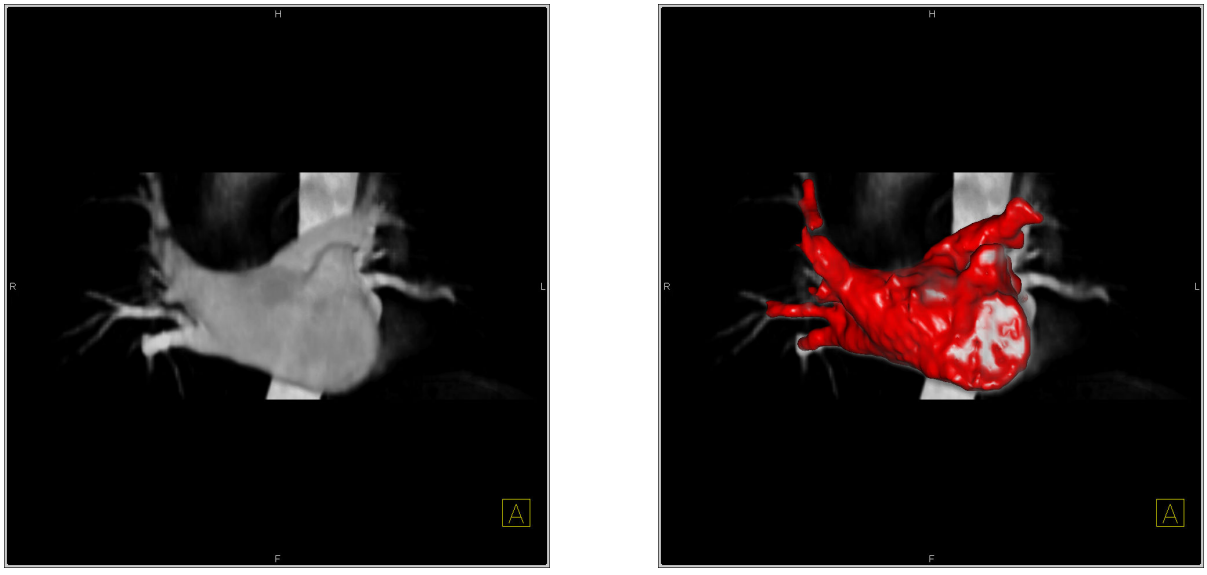

(a) (b)

Figure 2: *(a) MRI volume data of the left atrium. (b) The same volume data set combined with the segmentation of the left atrium. The segmentation was performed using syngo InSpace EP (Siemens AG, Healthcare Sector, Forchheim, Germany).*

will appear as an image pixel. To realize the carving effect, only the front faces of the LA are affected. The decision, whether a pixel of the mesh is visible or discarded depends on the pixel's relative distance to the viewing position, which is set by the user. Before a pixel can be rejected, some information needs to be known. Besides the user-set carve factor $\rho_f \in [0,\ldots,1]$, which defines the degree of carving, the camera position $\mathbf{p}_c \in \mathbb{R}^3$ needs to be known as well. In addition, the maximum distance of a pixel to the origin $d_{\max} \in \mathbb{R}$ is

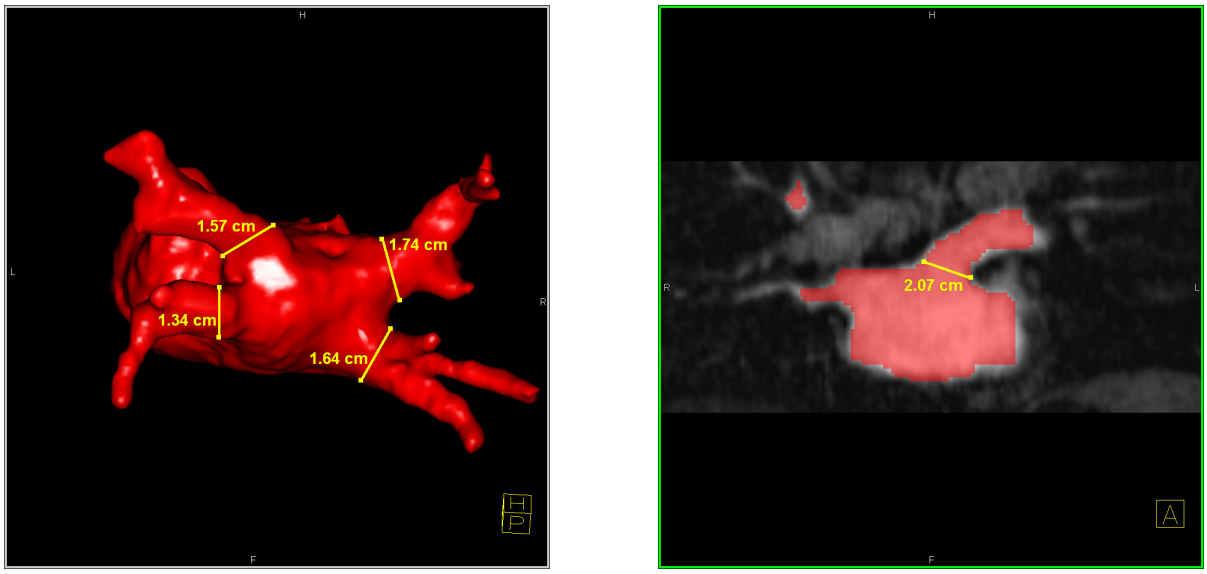

(a) (b)

Figure 3: *(a) Assessment of the diameter of the four pulmonary veins by considering only the segmentation result. (b) Assessment of the diameter of one pulmonary vein by considering the combination of the segmentation and the pre-operative data set.*

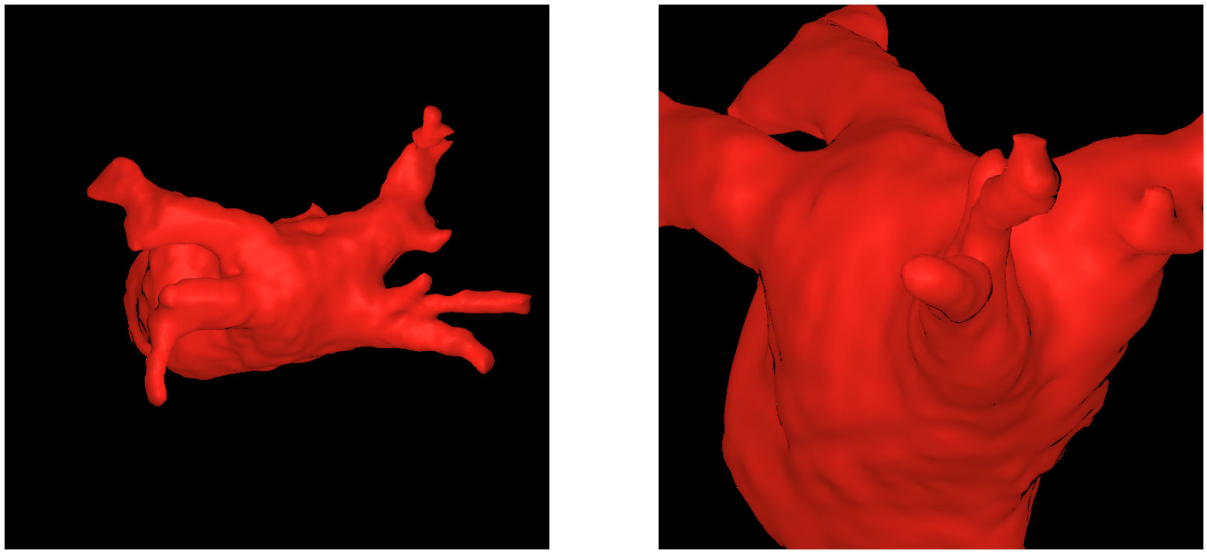

(a) (b)

Figure 4: *(a) Visualization of the left atrium. (b) Visualization of the left atrium after rotation and zoomed in.*

estimated by

$$d_{\max} = \max_i ||\mathbf{p}_i||_2 \quad (1)$$

with the mesh vertices $\mathbf{p}_i \in \mathbb{R}^3$. An illustration of the orthographic projection and the distances required for the calculation of the carving is given in Fig. 6. The position of a mesh vertex $\mathbf{p}_i$, with $i \in \mathbb{N}$ the number of mesh vertices, is known. In our case, N is about 20.000. This distance is calculated

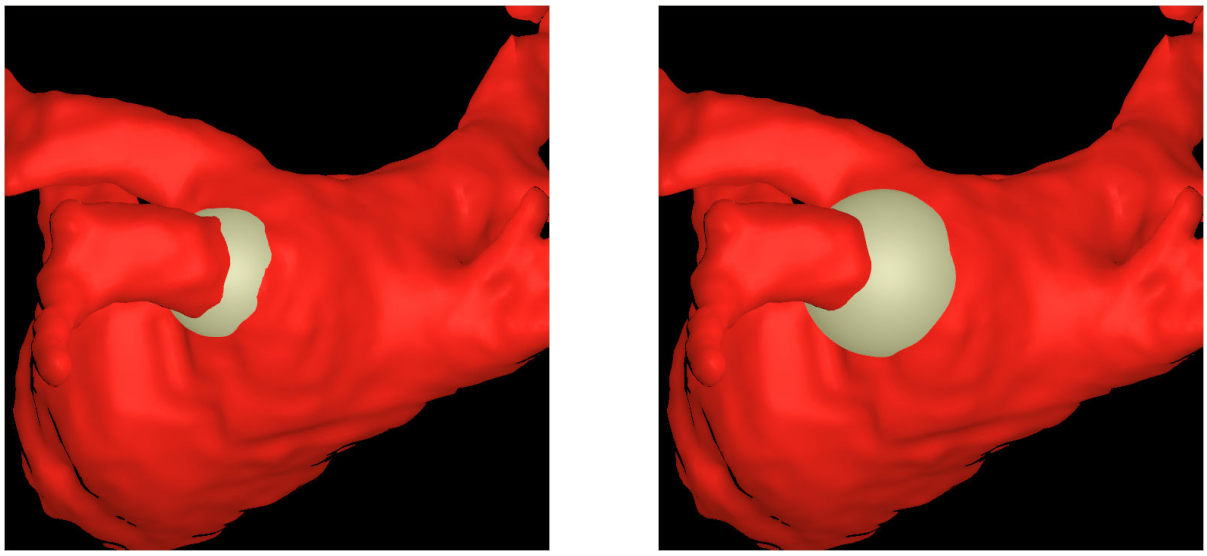

(a) (b)

Figure 5: *(a) Visualization of the 23 mm balloon positioned at the left inferior pulmonary vein. (b) The same pulmonary vein with a 28 mm balloon at the same position.*

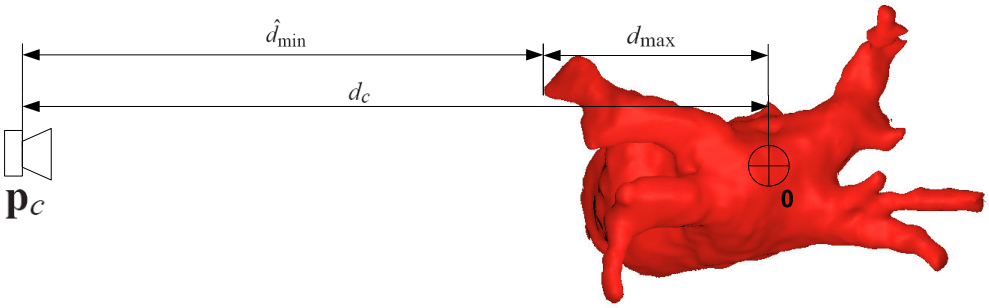

Figure 6: *Illustration of the orthographic projection and the distances used for carving. The maximum distance $d_{\max}$ of a mesh vertex to the origin is calculated only once during mesh loading. The minimum distance $\hat{d}_{\min}$ of a mesh vertex to the camera is estimated by the subtraction of $d_{\max}$ from d_c, with the distance of the camera to the origin as d_c.*

only once while the left atrium is loaded. Since the mesh is centered at the origin, it is sufficient to calculate the norm of each loaded vertex and store only the vertex with the maximal distance. As previously mentioned, the left atrium is centered around the origin and an orthographic projection is used. Thus, the maximal distance $d_c \in \mathbb{R}$ that a front facing pixel can have to the camera, is equal to the distance between the camera and the origin, which is given as

$$d_c = ||\mathbf{p}_c||_2. \tag{2}$$

Next, the minimum distance between a front facing pixel and the camera has to be determined. Since this distance depends on the current geometrical shape of the LA, we approximate this distance by calculating the overall minimal distance $\hat{d}_{\min} \in \mathbb{R}$. As d_c is known, we can derive

$$\hat{d}_{\min} = d_c - d_{\max}. \tag{3}$$

In camera space, the distance $d(\mathbf{q}_j) \in \mathbb{R}$ between the current processed mesh pixel $\mathbf{q}_j \in \mathbb{R}^3$, with $j \in \mathbb{N}$ and the camera center is determined as

$$d(\mathbf{q}_j) = ||\mathbf{q}_j||_2. \tag{4}$$

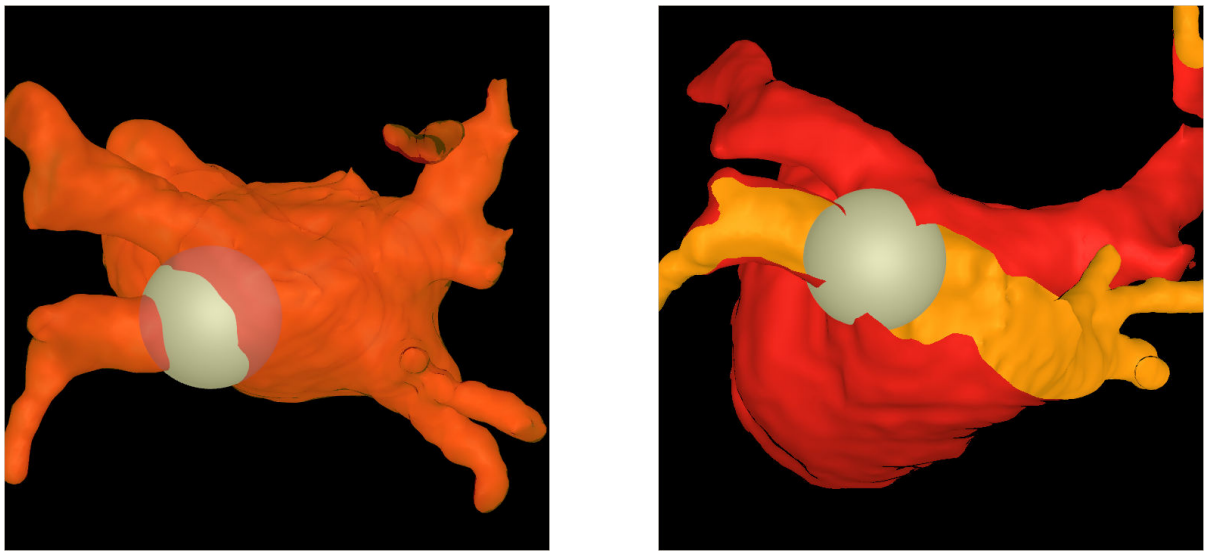

(a) (b)

Figure 7: *(a) Visualization of the transparency effect. (b) Carving view of the pulmonary vein with a cryo-balloon in place. The front-face of the left atrium is colored in red, the back-face in amber and the cryo-balloon in gray.*

The ratio $\rho \in \mathbb{R}$ that describes the relative distance of a mesh pixel is obtained by

$$\rho = \frac{|d(\mathbf{q}_j) - \hat{d}_{min}|}{d_{max}}. \quad (5)$$

A comparison of ρ with the current carve factor ρ_f is used to decide whether a vertex shall be discarded or not. An example of the visualization is given in Fig. 7 (b). As the maximal distance of a vertex to the origin is calculated only once, our method requires only one rendering pass. This approach is similar to the importance driven visualization proposed in [VKG04, VKG05]

4. Discussion and Conclusions

Using AFiT, a physician can get direct 3-D visual feedback to determine which type of cryo-balloon catheter should be used for the procedure. The visualization is performed using a segmented left atrium. The first feedback obtained from electrophysiologists, who were involved in the development of AFiT, was very encouraging. Our proposed tool is easy to use and the visualization helps to find the correct balloon catheter for the procedure. Nevertheless, more feedback and a clinical evaluation are needed to quantify the clinical impact of this new planning tool. Still, since AFiT provides interactive visualization features to explore how a cryo-balloon can be deployed in 3-D, we expect that physicians will use this tool to determine if a cryo-balloon ablation strategy makes sense for the LA anatomy at hand.

The current limitation of AFiT is that we do not provide any feedback about wall contact. This has to be assessed manually by the physician. Deformation of the LA up to a certain extent may be beneficial. In addition to that, our catheter models can currently be placed literally anywhere even if the position is not directly accessible. Feedback should be provided automatically if the catheter can be positioned at the planned position or not.

Apart from that, one could assess the clinical value using a study where a certain number of cases is performed without and using the tool. There may be a difference in procedure time and possibly even outcome. Further research will focus on making the planned cryo-balloon positions part of the live fluoroscopic images employing augmented fluoroscopy techniques. A first approach to reconstruct a balloon-catheter during the procedure within a pre-operative data set is presented in [KBB*11]. The value of fluoroscopic overlay images for radio-frequency catheter ablations has been proven [EDH*08, DME*05, BLHS09, BWL*10, BLSH10, BLHS10]. An extension of AFiT to cover other single-shot devices, such as the *pulmonary vein ablation catheter* (PVAC, Medtronic Ablation Frontiers LLC, Carlsbad, CA, USA), or the *multi-array ablation catheter* (MAAC, Medtronic Ablation Frontiers LLC, Carlsbad, CA, USA) is also conceivable. Focusing on intra-procedural visualization, catheters as the force-sensing catheter are also of interest [KLK*11]. Further extension could also focus on different interventions, such as transcatheter aortic valve implantation [SKH*11] or stent placements [RES*07, RPS*09, ZJL*10, JLZ*10]. In general, one could say, our tool could help whenever a 3-D device needs

to be placed and the diameter of the device has to be determined beforehand.

Acknowledgements

This work has been supported by the German Federal Ministry of Education and Research in the context of the initiative Spitzencluster Medical Valley - Europäische Metropolregion Nürnberg. Additional funding was provided by Siemens AG.

References

[AHH08] AKENINE-MOLLER T., HAINES E., HOFFMAN N.: *Real-Time Rendering*, third ed. AK Peters, Natick, MA, USA, July 2008. 2

[AUR*03] AVITALL B., URBONIENE D., ROZMUS G., LAFONTAINE D., HELMS R., URBONAS A.: New Cryotechnology for Electrical Isolation of the Pulmonary Veins. *Journal of Cardiovascular Electrophysiology 14*, 3 (2003), 281–286. 1

[BBLP10] BLANKE P., BAUMANN T., LANGER M., PACHE G.: Imaging of pulmonary vein anatomy using low-dose prospective ecg-triggered dual-source computed tomography. *Eur Radiol 20* (2010), 1851–1855. 2

[BBY*10] BOURIER F., BROST A., YATZIV L., HORNEGGER J., STROBEL N., KURZIDIM K.: Coronary Sinus Extraction for Multimodality Registration to guide Transseptal Puncture. In *8th Interventional MRI Symposium - Book of Abstracts* (2010), Kahn T., Jolesz F., Lewin J., (Eds.), pp. 311–313. 1

[BHS*11] BOURIER F., HEISSENHUBER F., SCHNEIDER H.-J., GANSLMEIER P., FISCHER R., BROST A., KOCH M., STROBEL N., HORNEGGER J., KURZIDIM K.: 3D-Funktionalität und Navigation durch einen Siemens-Prototypen in der biplanen Fluoroskopie zur Pulmonalvenenisolation. *Clin Res Cardiol 100*, Suppl 1 - V186 (April 2011). 1

[BLHS09] BROST A., LIAO R., HORNEGGER J., STROBEL N.: 3-D Respiratory Motion Compensation during EP Procedures by Image-Based 3-D Lasso Catheter Model Generation and Tracking. In *Lect. Notes Comput. Sci.* (London, 2009), Yang G., Hawkes D., Rueckert D., Noble J., Taylor C., (Eds.), vol. 5761, pp. 394–401. 6

[BLHS10] BROST A., LIAO R., HORNEGGER J., STROBEL N.: Model-Based Registration for Motion Compensation during EP Ablation Procedures. In *Biomedical Image Registration*, Fischer B., Dawant B., Lorenz C., (Eds.), vol. 6204 of *LNCS*. Springer Berlin / Heidelberg, 2010, pp. 234–245. 6

[BLSH10] BROST A., LIAO R., STROBEL N., HORNEGGER J.: Respiratory motion compensation by model-based catheter tracking during EP procedures. *Medical Image Analysis 14*, 5 (2010), 695–706. Special Issue on the 12th International Conference on Medical Image Computing and Computer-Assisted Intervention (MICCAI) 2009. 6

[BSG*11] BOURIER F., SCHNEIDER H.-J., GANSLMEIER P., HEISSENHUBER F., FISCHER R., BROST A., KOCH M., STROBEL N., HORNEGGER J., KURZIDIM K.: Unterstuetzung der transseptalen Punktion durch vorherige Überlagerung eines 3D-Volumens von linkem Atrium und Aorta. *Clin Res Cardiol 100*, Suppl 1 - P710 (April 2011). 1

[BSH*11] BOURIER F., SCHNEIDER H.-J., HEISSENHUBER F., GANSLMEIER P., FISCHER R., BROST A., KOCH M., STROBEL N., HORNEGGER J., KURZIDIM K.: Frühzeitige Registrierung eines 3D-Overlays des linken Atriums während linksatrialen Ablationen mittels Koronarsinuskatheter. *Clin Res Cardiol 100*, Suppl 1 - V522 (April 2011). 1

[BSY*09a] BROST A., STROBEL N., YATZIV L., GILSON W., MEYER B., HORNEGGER J., LEWIN J., WACKER F.: Accuracy of x-ray image-based 3D localization from two C-arm views: a comparison between an ideal system and a real device. In *SPIE Medical Imaging 2009: Visualization, Image-Guided Procedures, and Modeling* (Lake Buena Vista, FL, USA, February 2009), Miga M. I., Wong K. H., (Eds.), vol. 7261, p. 72611Z. 2

[BSY*09b] BROST A., STROBEL N., YATZIV L., GILSON W., MEYER B., HORNEGGER J., LEWIN J., WACKER F.: Geometric Accuracy of 3-D X-Ray Image-Based Localization from Two C-Arm Views. In *Workshop on Geometric Accuracy In Image Guided Interventions - Medical Image Computing and Computer Assisted Interventions 2009* (London UK, September 2009), Joskowicz L., Abolmaesumi P., Fitzpatrick M., (Eds.), MICCAI, pp. 12–19. 2

[BWL*10] BROST A., WIMMER A., LIAO R., HORNEGGER J., STROBEL N.: Catheter Tracking: Filter-Based vs. Learning-Based. In *Pattern Recognition*, Goesele M., Roth S., Kuijper A., Schiele B., Schindler K., (Eds.), vol. 6376 of *LNCS*. Springer Berlin / Heidelberg, 2010, pp. 293–302. 6

[BWL*11] BROST A., WIMMER A., LIAO R., HORNEGGER J., STROBEL N.: Constrained 2-D/3-D Registration for Motion Compensation in AFib Ablation Procedures. In *IPCAI 2011, Berlin, Germany*, vol. 6689 of *LNCS*. Springer Berlin / Heidelberg, 2011, pp. 133–144. 1

[CAMO11] CLAYVILLE L., ANDERSON K., MILLER S., ONGE E.: New options in Anticoagulation for the Prevention Of Venous Thromboembolism and Stroke. *Pharmacy and Therapeutics 36*, 2 (February 2011), 86–99. 1

[CBP*07] CALKINS H., BRUGADA J., PACKER D., CAPPATO R., CHEN S., CRIJNS H., DAMIANO R., DAVIES D., HAINES D., HAÏSSAGUERRE M., IESAKA Y., JACKMAN W., JAIS P., KOTTKAMP H., KUCK K., LINDSAY B., MARCHLINSKI F., MCCARTHY P., MONT J., MORADI F., NADEMANEE K., NATALE A., PAPPONE C., PRYSTOWSKY E., RAVIELE A., RUSKIN J., SHEMIN R.: HRS/EHRA/ECAS Expert Consensus Statement on Catheter and Surgical Ablation of Atrial Fibrillation: Recommendations for Personnel, Policy, Procedures and Follow-Up. *Heart Rhythm 4*, 6 (Jun. 2007), 1–46. 1

[DKCJ11] DEFAYE P., KANE A., CHAIB A., JACON P.: Efficacy and safety of pulmonary vein isolation by cryoablation for the treatment of paroxysmal and persistend atrial fibrillation. *Europace* (March 2011), [Epub ahead of print]. 1

[DME*05] DE BUCK S., MAES F., ECTOR J., BOGAERT J., DYMARKOWSKI S., HEIDBÜCHEL H., SUETENS P.: An augmented reality system for patient-specific guidance of cardiac catheter ablation procedures. *IEEE Trans. Med. Imaging 24*, 11 (2005), 1512–1524. 1, 6

[EDDL*08] ECTOR J., DE BUCK S., D. LOECKX W. C. F. M., DYMARKOWSKI S., BOGAERT J., HEIDBÜCHEL H.: Changes in Left Atrial Anatomy Due to Respiration: Impact on Three-Dimensional Image Integration During Atrial Fibrillation Ablation. *J Cardiovasc. Electr. 19*, 7 (2008), 828–834. 1

[EDH*08] ECTOR J., DE BUCK S., HUYBRECHTS W., NUYENS D., DYMARKOWSKI S., BOGAERT J., MAES F., HEIDBÜCHEL H.: Biplane three-dimensional augmented fluoroscopy as single navigation tool for ablation of atrial fibrillation: Accuracy and clinical value. *Heart Rhythm 5*, 7 (Mar. 2008), 957–964. 1, 6

[FO11] FÜRNKRANZ A., OUYANG F.: Non-invasive imaging prior to cryoballoon ablation of atrial fibrillation: what can we learn? *Europace 13* (2011), 153–154. 1, 2

[FR11] FULLER C., REISMAN M.: Stroke Prevention in Atrial Fibrillation: Atrial Appendage Closure. *Curr Cardiol Rep [Epub ahead of print]* (2011), n/a. 1

[GWS*01] GAGE B., WATERMAN A., SHANNON W., BOECHLER M., RICH M., RADFORD M.: Validation of Clinical Classification Schemes for Predicting Stroke. *JAMA 285*, 22 (June 13 2001), 2864–2870. 1

[HGF*94] HAISSAGUERRE M., GENCEL L., FISCHER B., LE METAYER P., POQUET F., MARCUS F., CLEMENTY J.: Successful Catheter Ablation of Atrial Fibrillation. *J Cardiovasc Electrophysiol 5* (1994), 1045–1052. 1

[JLZ*10] JOHN M., LIAO R., ZHENG Y., NÖTTLING A., BOESE J., KIRSCHSTEIN U., KEMPFERT J., WALTHER T.: System to guide transcatheter aortic valve implantations based on interventional c-arm ct imaging. In *Proceedings of the 13th international conference on Medical image computing and computer-assisted intervention: Part I* (Berlin, Heidelberg, 2010), MICCAI'10, Springer-Verlag, pp. 375–382. 6

[KBB*11] KLEINOEDER A., BROST A., BOURIER F., KOCH M., KURZIDIM K., HORNEGGER J., STROBEL N.: Cryo-Balloon Reconstruction from Two Views. *International Conference on Image Processing* (September 2011), [accepted]. 6

[KLK*11] KOCH M., LANGENKAMP A., KIRALY A., BROST A., STROBEL N., HORNEGGER J.: Navigation System with Contact Force Assessment to Guide Pulmonary Vein Isolation Procedures. In *23rd Conference of the Society for Medical Innovation and Technology* (Sept. 13 – 16 2011), p. [accepted]. 6

[MHB*03] MIQUEL M. E., HILL D. L. G., BAKER E. J., QURESHI S. A., SIMON R. D. B., KEEVIL S. F., RAZAVI R. S.: Three- and four-dimensional reconstruction of intracardiac anatomy from two-dimensional magnetic resonance images. *The International Journal of Cardiovascular Imaging 19* (2003), 239–254. 2

[NVS*08] NEUMANN T., VOGT J., SCHUMACHER B., DORSZEWKSI A., KUNISS M., NEUSER H., KURZIDIM K., BERKOWITSCH A., KOLLER M., HEINTZE J., SCHOLZ U., WETZEL U., SCHNEIDER M., HORSTKOTTE D., HAMM C., PITSCHNER H.: Circumferential Pulmonary Vein Isolation With the Cryoballoon Technique. *Journal of the American College of Cardiology 52*, 4 (2008), 273 – 278. 1

[PHL*09] PRÜMMER M., HORNEGGER J., LAURITSCH G., WIGSTRÖM L., GIRARD-HUGHES E., FAHRIG R.: Cardiac C-arm CT: a unified framework for motion estimation and dynamic CT. *IEEE Trans Med Imaging 28*, 11 (November 2009), 1836–1849. 1, 2

[RES*07] RICHTER G., ENGELHORN T., STRUFFERT T., DOELKEN M., GANSLANDT O., HORNEGGER J., KALENDER W. A., DOERFLER A.: Flat panel detector angiographic ct for stent-assisted coil embolization of bread-based cerebral aneurysms. *AJNR Am J Neuroradiol 28* (2007), 1902–1908. 6

[RLG*09] ROST R., LICEA-KANE B., GINSBURG D., KESSENICH J., LICHTENBELT B., MALAN H., WEIBLEN M.: *OpenGL Shading Language*, third ed. Addison-Wesley Professional, July 2009. 2

[RPS*09] RICHTER G., PFISTER M., STRUFFERT T., ENGELHORN T., DOELKEN M., SPIEGEL M., HORNEGGER J., DOERFLER A.: Technical feasibility of 2d-3d coregistration for visualization of self-expandable microstents to facilitate coil empolization of broad-based intracranial aneurysms: an in vitro study. *Neuroradiology 51* (2009), 851–854. 6

[Shr09] SHREINER D.: *OpenGL Programming Guide: The Official Guide to Learning OpenGL*, 7th ed. Addison-Wesley Professional, July 2009. 2

[SKH*11] SCHOENHAGEN P., KAPADIA S. R., HALLIBURTON S. S., SVENSSON L. G., TUZCU E. M.: Computed tomography evaluation for transcatheter aortic valve implantation (tavi): Imaging of the aortic root and iliac arteries. *Journal of Cardiovascular Computed Tomography In Press, Corrected Proof* (2011), –. 6

[SMB*09] STROBEL N., MEISSNER O., BOESE J., BRUNNER T., HEIGL B., HOHEISEL M., LAURITSCH G., NAGEL M., PFISTER M., RÜHRNSCHOPF E.-P., SCHOLZ B., SCHREIBER B., SPAHN M., ZELLERHOFF M., KLINGENBECK-REGN K.: Imaging with Flat-Detector C-Arm Systems. In *Multislice CT (Medical Radiology / Diagnostic Imaging)*, Reiser M. F., Becker C. R., Nikolaou K., Glazer G., (Eds.), third ed. Springer Berlin / Heidelberg, January 2009, ch. 3, pp. 33–51. 2

[VJR*07] VAN BELLE Y., JANSE P., RIVERO-AYERZA M., THORNTON A., JESSURUN E., THEUNS D., JORDAENS L.: Pulmonary vein isolation using an occluding cryoballoon for circumferential ablation: feasibility, complications, and short-term outcome. *European Heart Journal für Kardiologie 28* (2007), 2231 – 2237. 1

[VKG04] VIOLA I., KANITSAR A., GRÖLLER M. E.: Importance-driven volume rendering. In *In Proceedings of IEEE Visualization* (2004), pp. 139–145. 6

[VKG05] VIOLA I., KANITSAR A., GRÖLLER M. E.: Importance-driven feature enhancement in volume visualization. *IEEE Trans. Vis. Comput. Graph. 11*, 4 (2005), 408–418. 6

[WAK91] WOLF P., ABBOTT R., KANNEL W.: Atrial fibrillation as an independent risk factor for stroke: the Framingham Study. *Stroke 22* (1991), 983–988. 1

[WHSL10] WRIGHT R., HAEMEL N., SELLERS G., LIPCHAK B.: *OpenGL SuperBible*, 5th ed. Addison-Wesley Professional, August 2010. 2

[ZJL*10] ZHENG Y., JOHN M., LIAO R., BOESE J., KIRSCHSTEIN U., GEORGESCU B., ZHOU S. K., KEMPFERT J., WALTHER T., BROCKMANN G., COMANICIU D.: Automatic aorta segmentation and valve landmark detection in c-arm ct: application to aortic valve implantation. In *Proceedings of the 13th international conference on Medical image computing and computer-assisted intervention: Part I* (Berlin, Heidelberg, 2010), MICCAI'10, Springer-Verlag, pp. 476–483. 6